

A Primary Evaluation of Potential Small-Molecule Inhibitors of the Astacin Metalloproteinase Ovastacin, a Novel Drug Target in Female Infertility Treatment**

Hagen Körschgen,^[a] Christian Jäger,^[b] Kathrin Tan,^[b] Mirko Buchholz,^[b] Walter Stöcker,^{*,[a]} and Daniel Ramsbeck^{*,[b]}

Despite huge progress in hormonal therapy and improved *in vitro* fertilization methods, the success rates in infertility treatment are still limited. A recently discovered mechanism revealed the interplay between the plasma protein fetuin-B and the cortical granule-based proteinase ovastacin to be a novel key mechanism in the regulation of fertilization. Upon sperm-egg fusion, cleavage of a distinct zona pellucida component by ovastacin destroys the sperm receptor, enhances zona robustness, and eventually provides a definitive block against polyspermy. An untimely onset of this zona hardening prior to fertilization would consequently result in infertility. Physiologically, this process is controlled by fetuin-B, an endogenous ovastacin inhibitor. Here we aimed to discover small-molecule inhibitors of ovastacin that could mimic the effect of fetuin-B. These compounds could be useful lead structures for the development of specific ovastacin inhibitors that can be used in infertility treatment or *in vitro* fertilization

During mammalian fertilization, sperm entry into the ovum is tightly regulated. Dysregulation of this finely tuned process promotes infertility. An essential mechanism at this point is the inhibition of ovastacin, a member of the astacin family and the metzincin superfamily of metalloproteinases.^[1] Upon fertilization, the release of ovastacin (encoded by the gene *astl*) from the oocyte's cortical granules into the perivitelline space leads to remodeling of the zona pellucida (ZP), a glycoprotein matrix

surrounding the oocyte, by cleavage of the zona pellucida protein 2 (ZP2) at a distinct site. This cleavage abolishes sperm binding, renders the ZP impermeable and thus blocks further sperm to enter the oocyte.^[2] However, even before fertilization, during oocyte maturation, small amounts of ovastacin seep out of the oocyte to cause zona pellucida hardening.^[3] Under physiological conditions, pre-fertilization cleavage of ZP2 is inhibited by the plasma protein fetuin-B, a very potent and specific endogenous inhibitor of ovastacin.^[4,5] As shown recently, the absence of fetuin-B causes infertility in knock-out mice due to this prefertilization cleavage.^[6] Hence, this proteolytic network comprising zona pellucida components (i.e., ZP2), ovastacin, and the inhibitor fetuin-B is an important mechanism in the regulation of female fertility. About 5% of all couples are affected by infertility and the unfulfilled desire of having children.^[7] Current treatment usually involves several hormones or other peptidic drugs and *in vitro* fertilization (IVF). Addition of fetuin-B increases the fertilization rate *in vitro* in mice^[8] and even in human serum fetuin-B levels correlate with the outcome of IVF.^[9] This points out the importance of the regulation of ovastacin during fertilization. However, despite the high inhibitory potency of fetuin-B, its application in infertility treatment or IVF might be limited due to its proteinogenic origin, as well as the lack of well-defined fetuin-B containing IVF media.

In this setting, the inhibition of ovastacin by synthetic small molecules could be a valuable nonhormonal option for treating female infertility or an alternative supplement to facilitate IVF. Ovastacin is a member of the astacin-family within the metzincin superfamily of zinc-metalloproteinases, comprising ovastacin, meprin α/β and BMP-1/tolloid-like proteinases (BTPs) in humans.^[1] The BTPs have been in focus of drug development for fibrotic diseases and also the meprins are emerging drug targets, which led to the development of potent inhibitors, recently.^[10,11,12] However, except for the endogenous inhibitor fetuin-B, no specific compounds that modulate ovastacin activity have been reported to date.^[4,5,13] Due to the unmet medical need of nonhormonal infertility treatment, also accompanied with a high social impact, we tried to discover small-molecule inhibitors of ovastacin that could serve as starting point or lead compounds for the development of such a treatment or as additives for culture media that could facilitate IVF.

As mentioned above, inhibitors of other human astacin proteinases have already been reported and also the structures of mature BMP-1 and meprin β have been elucidated

[a] Dr. H. Körschgen, Prof. Dr. W. Stöcker
Institute of Molecular Physiology, Cell and Matrix Biology
Johannes Gutenberg University Mainz
Johann-Joachim-Becher-Weg 7
55128 Mainz (Germany)
E-mail: stoecker@uni-mainz.de

[b] C. Jäger, K. Tan, Dr. M. Buchholz, Dr. D. Ramsbeck
Department of Drug Design and Target Validation MWT
Fraunhofer Institute for Cell Therapy and Immunology IZI
Biocenter, Weinbergweg 22
06120 Halle (Saale) (Germany)
E-mail: daniel.ramsbeck@izi.fraunhofer.de

[**] A previous version of this manuscript has been deposited on a preprint server (<https://doi.org/10.26434/chemrxiv.11306867.v1>).

Supporting information for this article is available on the WWW under <https://doi.org/10.1002/cmdc.202000397>

© 2020 The Authors. Published by Wiley-VCH Verlag GmbH & Co. KGaA. This is an open access article under the terms of the Creative Commons Attribution Non-Commercial NoDerivs License, which permits use and distribution in any medium, provided the original work is properly cited, the use is non-commercial and no modifications or adaptations are made.

earlier.^[14,15] However, no structural data of meprin α and ovastacin is available to date. Thus, a homology model of human ovastacin was generated to compare the active sites of all human astacin proteinases to gain insight into structural similarities and differences that could guide compound selection for an inhibitor screening against ovastacin (Figure 1).

Although all astacin proteinases share a common fold, distinct differences within the active sites, that is, S_1 , S_1' and S_2'

lead to altered substrate specificities.^[1] However, these small structural differences could also lead to different preferred interactions that could be addressed for the design of selective inhibitors (Figure 2). The S_1 subsite is different in all the compared human astacin proteases. Thus, interactions with these residues, as proposed for the reported meprin inhibitors^[11,12] might be a major determinant of inhibitor activity and particularly their selectivity. While the S_1 site is shaped by

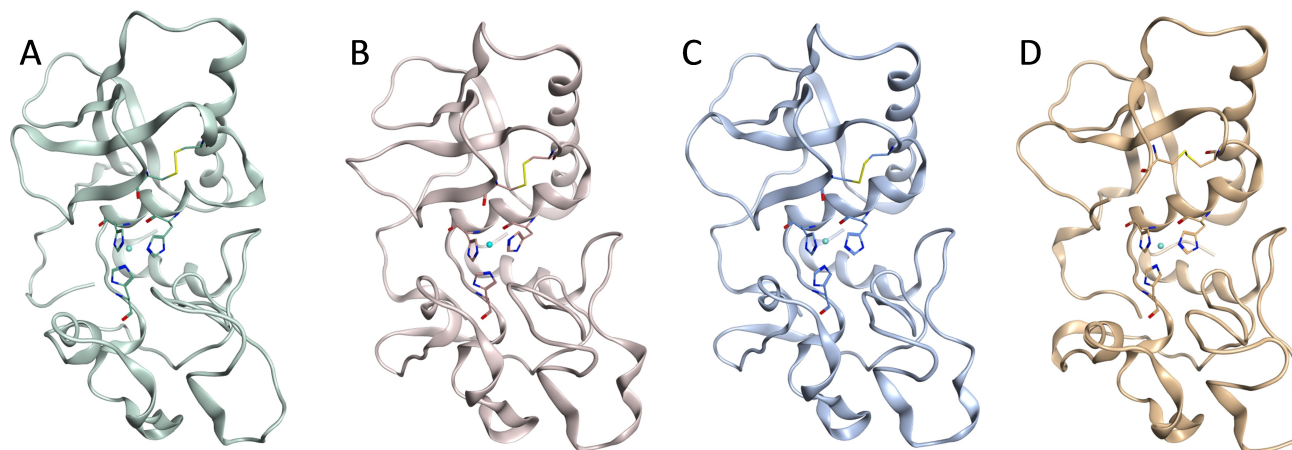


Figure 1. Comparison of the protease domains of A) human ovastacin (homology model), B) human meprin α (homology model), C) human meprin β (PDB ID: 4GWN) and D) human BMP-1 (PDB ID: 3EDG).

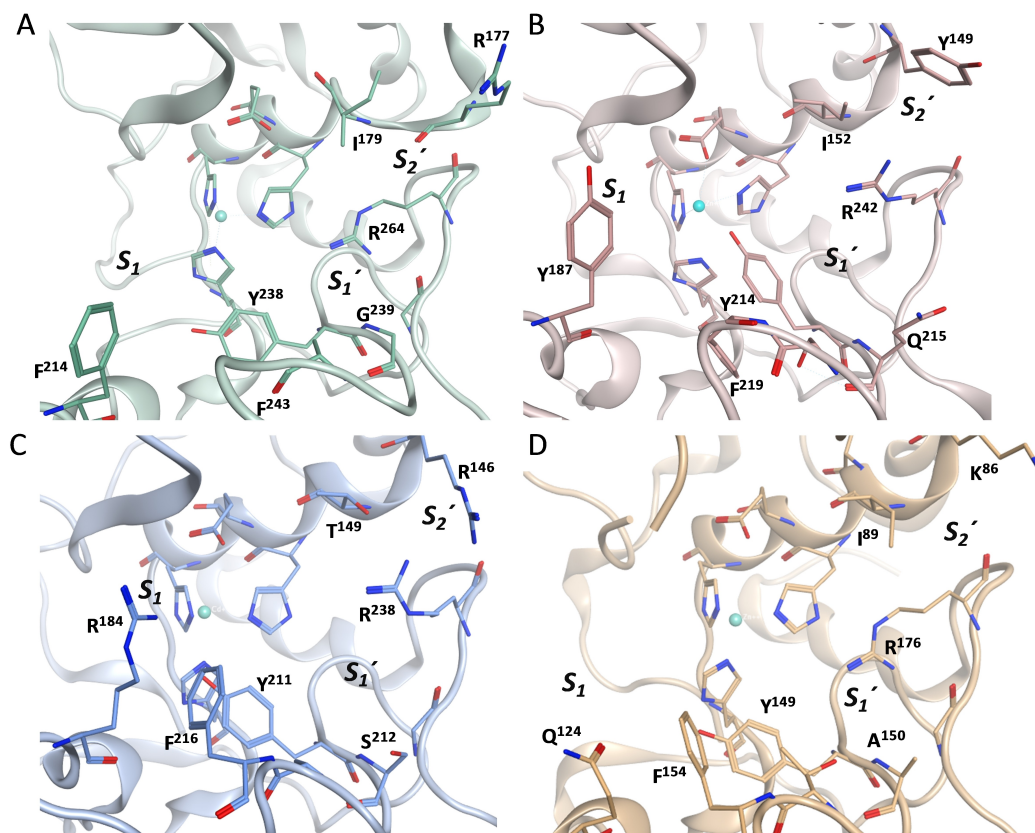


Figure 2. Detailed view of the active sites. A) human ovastacin, B) hmeprin α , C) hmeprin β , and D) hBMP-1. The side chains of amino acids within the active sites that are potentially involved in ligand binding are highlighted.

Phe214 in ovastacin, the respective residue is Tyr187 in meprin α , Arg184 in meprin β and Gln124 in BMP-1, respectively. Hence, the S_1 site of ovastacin is much more lipophilic compared to the polar environment in meprin β or BMP-1 and thus more similar to the physicochemical character of tyrosine, as found in meprin α . The amino acids shaping the S_1' subpocket are highly conserved among the astacins. The respective arginine residues, Arg264 in ovastacin, Arg242 in meprin α , Arg238 in meprin β and Arg176 in BMP-1 are the major contributors to the preference for acidic amino acids in P_1' position of the astacin proteinase substrates.^[16]

However, some amino acids flanking the S_1' site are different. While Gln215 in meprin α or Ser212 in meprin β could be involved in hydrogen bonds contributing to ligand binding, the respective residues—Gly239 in ovastacin and Ala150 in BMP-1—rule out electrostatic side-chain interactions. The S_2' site is again quite similar among the compared proteinases, featuring a hydrophilic, basic environment created by Arg177 in ovastacin, Arg146 in meprin β and Lys86 in BMP-1. Only meprin α exhibits a different pattern, with Tyr149 creating a more lipophilic environment in the S_2' pocket. Taken together, the residues within the active site of ovastacin share some features of meprin α as well as meprin β , but differ slightly from BMP-1.

Due to the structural similarities that could contribute to inhibitor interactions, in particular within the S_1 , S_1' and S_2' subsites of ovastacin with either meprin α and β , we assumed that the recently reported tertiary amine based hydroxamate inhibitors might also be able to inhibit the activity of ovastacin. The expression and purification of human ovastacin has proven not to be useful due to worse purity and low activity, yet. Thus, the development of potential inhibitors is hampered. However, murine and human ovastacin share an overall sequence identity of ~68%. Moreover, within the active site cleft the residues shaping the subsites that are assumed to be involved in inhibitor binding, that is, S_1 , S_1' , and S_2' , are virtually identical with a sequence identity of ~97%. Just one residue adjacent to the S_2' pocket differs significantly: Arg174 in murine ovastacin versus Gln174 in the human enzyme (see sequence alignment and structural comparison in the Supporting Information). However, this might not contribute to the binding of small-molecule inhibitors targeting the catalytic Zn^{2+} ion as primary interaction, which for astacin metalloproteinases was first studied with transition-state analogue inhibitors directed against prototypal astacin^[17] and hydroxamates targeting meprins.^[18] Small structural differences within the active sites of murine and human ovastacin revealed by the homology models might be attributed to the individual model quality, albeit both used the same structural template and thus might be negligible. However, in the present model of murine ovastacin, Ile179 is swung out towards the upper rim of the active site cleft. In the model of human ovastacin, Phe243 is turned away from the catalytic center, although in all available structures of astacins and the remaining homology models, the respective residue is involved in shaping the lower rim of the active-site cleft. Thus, the orientation of the side chains of some active site residues in murine and human ovastacin remains elusive and could be solved by X-ray crystallography in the future. Never-

theless, readily available murine ovastacin is suitable for an initial focused inhibitor screen. Hence, selected potent meprin α and meprin β inhibitors reported previously (1–9),^[11,12] covering a range of different structural features, were screened against murine ovastacin to probe their potential as lead compounds for drug development and further compound optimization (Table 1).

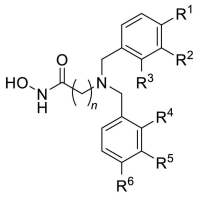
The evaluation of the inhibitory potency against murine ovastacin revealed a dose dependent reduction of ovastacin activity by all of the tested compounds. Furthermore, the majority of compounds exhibited a significant inhibition, that is, a relative activity < 50% at a compound concentration of 5 μ M (see the Supporting Information).

Obviously, compounds that are preferably inhibitors of meprin β (1, 5, 8, 9) exhibit slightly less inhibitory activity against murine ovastacin compared to compounds with higher activity against meprin α (4 and 6, the respective data for meprin α and β can be found in the Supporting Information). Notably, the latter two are derivatives of β -alanine, whereas the remaining compounds are glycine hydroxamates, which exhibit shorter spacers. The same influence of the spacer length was already observed for meprin α versus meprin β activity and is further corroborated by compound 2, exhibiting also a slightly higher activity compared to 1.^[12]

Although the homology models do not reveal differences in the overall geometry of the active site, there seem to exist slight differences in the native conformation of ovastacin compared to meprin β , that lead to the same preference of β -alanine derived inhibitors as for meprin α , but remains elusive with the present models. Furthermore, compounds 1, 2, 7, 8 and 9 bear at least one carboxylic acid moiety. Although the S_1' and S_2' pockets of ovastacin are shaped by arginines and almost all astacins exhibit the same preference for acidic P_1' residues, this moiety is obviously less favorable for inhibitor binding. This also corroborates the structure-activity relationships found for meprin α .^[12] This reduced activity could be due to the lack of a hydrogen bond donor within the S_1' site of ovastacin, that is, Gly239 versus Ser212 in meprin β , that additionally contributes to ligand binding, rather than solely a charged interaction with the arginine.

The most effective inhibition of ovastacin was observed for compound 6, which has a K_i^{app} value of 0.49 ± 0.06 μ M. Although, this compound is still a more potent inhibitor of meprin α and β (see the Supporting Information), it turned out to be a pan-specific astacin inhibitor, balancing lipophilicity with reduced acidity caused by the halophenol moieties, thereby enabling interactions with either lipophilic or basic S_1 , S_1' or S_2' subpockets found in ovastacin, meprin α or meprin β , respectively. However, regarding a potential utilization of ovastacin inhibitors for *in vitro* fertilization, high selectivity might not be necessary, as neither meprin α nor β is present in the physiological context of fertilization. Thus, 6 could be used as tool compound for further studies. Nevertheless, for a potential application *in vivo*, higher selectivity for ovastacin should be achieved to avoid side effects due to meprin α or β inhibition, that is, decreased tensile strength in the skin,

Table 1. Inhibition of murine ovastacin by tertiary amine hydroxamic acids.^[a]

							n	K_i^{app} [μM] ^[b]
	R ¹	R ²	R ³	R ⁴	R ⁵	R ⁶		
1	H	COOH	H	H	COOH	H	1	2.16 ± 0.02
2	H	COOH	H	H	COOH	H	2	1.06 ± 0.03
3	–OCH ₂ O–		H	H	–OCH ₂ O–		1	2.56 ± 0.13
4	–OCH ₂ O–		H	H	–OCH ₂ O–		2	1.15 ± 0.07
5	Cl	OH	F	F	OH	Cl	1	0.81 ± 0.37
6	Cl	OH	F	F	OH	Cl	2	0.49 ± 0.06
7	H	COOH	H	H	H	H	1	11.10 ± 0.89
8	H	COOH	H	H	H	OCH ₃	1	6.33 ± 0.31
9	H	COOH	H	H	–OCH ₂ O–		1	2.39 ± 0.06
10	Cl	H	F	F	H	Cl	2	2.13 ± 0.21
11	Cl	OCH ₃	F	F	OCH ₃	Cl	2	1.13 ± 0.09
12	Cl	H	F	F	OH	Cl	2	0.75 ± 0.04
13	Cl	OH	F	H	–OCH ₂ O–		2	0.68 ± 0.02
14	Cl	H	F	H	–OCH ₂ O–		2	1.96 ± 0.08
15	H	N _(pyridine)	H	H	–OCH ₂ O–		2	8.12 ± 0.34
16	H	N _(pyridine)	H	F	OH	Cl	2	3.13 ± 0.01
17	N _(pyridine)	N _(pyridine)	H	H	–OCH ₂ O–		2	7.58 ± 0.36
18	N _(pyridine)	H	H	F	OH	Cl	2	8.18 ± 0.29
19	H	N _(pyridine)	H	H	N _(pyridine)	H	2	28.30 ± 1.10
20	CN	H	H	H	H	CN	2	1.24 ± 0.37

[a] compounds 1–11, 19&20 have been reported previously;^[11,12] [b] mean ± SE of two independent experiments performed in triplicates

impaired barrier function or impaired intestinal mucin release.^[19]

The assumed interactions of **6** with the active site of ovastacin were corroborated by *in silico* docking. The majority of docking solutions revealed an orientation of the two halophenol moieties towards the S₁ and S₁' pockets (Figure 3, magenta). However, a clearly preferred conformation could not be observed, most likely due to the flexibility of the tertiary amines. Although, the top ranked docking solution (Figure 3, orange) suggests potential direct interactions with F214, F243 and R264 at the S₁ and S₁' sites. Nevertheless, these putative

interactions are just assumptions based on a homology model and have to be clarified by crystallographic experiments.

Based on these initial findings, further β -alanine hydroxamates (**10–20**) were evaluated with regard to their ovastacin inhibition. The depletion of the acidic phenols of **6**, leaving just an electron-deficient aryl moiety (**10**), led to a stronger decrease in activity, although it was less decreased by etherification of the phenol (**11**). However, the combination of an acidic halophenol with the electron-deficient chloro-fluoroaryl residue (**12**) again led to slightly increased inhibition of ovastacin. Also, the combination of the halophenol with an electron-rich

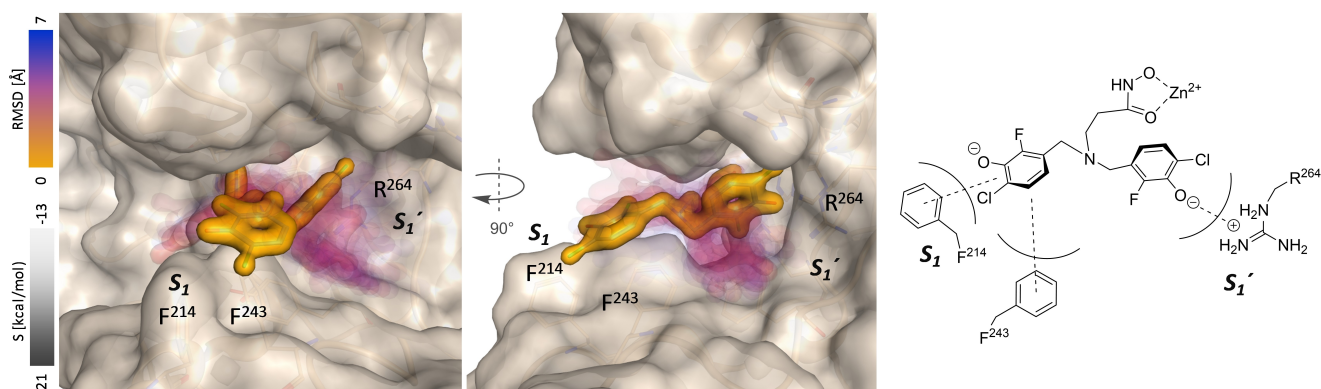


Figure 3. Proposed binding mode of **6** docked into the active site of murine ovastacin. Left and middle: Docking poses colored according to the RMSD compared to the top-ranked solution; increasing transparency indicates a lower docking score (visualization with PostDock); left: in standard orientation. Right: Schematic representation of potential interactions of the inhibitor (top-ranked docking solution) with the S₁ and S₁' pockets of murine ovastacin.

benzodioxolane moiety (**13**) led to pronounced inhibition of murine ovastacin. The depletion of the halophenol again led to a reduced activity of **14**, underpinning the importance of this polar substructure for favorable inhibition of ovastacin. The introduction of electron-deficient moieties, that is, pyridyl residues (**15–19**), as well as cyanoaryl (**20**), also led to significantly decreased inhibition of ovastacin.

This first insight into the structure–activity relationships of small-molecule ovastacin inhibitors exemplified the requirement of distinct features for specific and potent ovastacin inhibition, although the SAR of the screened inhibitors is rather flat and needs to be further explored. Nevertheless, this study revealed that inhibitors based on the tertiary amine hydroxamic acid scaffolds are also suitable inhibitors of ovastacin. This preliminary data resembles more the subsite specificity and structure–activity relationships found for meprin α , that is, a preference for lipophilic substituents and moieties with reduced acidity, rather than the polar carboxylic acid found to be important for potent and selective inhibition of meprin β . Assuming a similar binding mode as postulated for meprin α and β , this might be due to the higher similarity of ovastacin compared to meprin α within the respective binding pockets: the S_1' pocket, shaped by Arg264 and lacking an additional H-bond donor, like Ser212 in meprin β , and the S_1 pocket, shaped by Phe214 and Phe243, that creates a lipophilic binding site like Tyr187 in meprin α , rather than the polar cationic Arg184 in meprin β . Hence, the interaction with this subpocket might be the key element that could be addressed for the design of selective inhibitors of the individual proteinases. However, the structural elucidation of ovastacin in complex with an inhibitor will shed light on the true binding mode and potentially enable a structure-guided design of novel inhibitors.

In summary, this primary evaluation of tertiary amine hydroxamate-based compounds came up with the very first nanomolar small-molecule inhibitors of the astacin metalloproteinase ovastacin. Ovastacin catalyzes a unique and essential proteolytic cleavage within the egg envelope, which, under physiological conditions, is not performed by any other proteinase, as ZP2 remains uncleaved in ovastacin-deficient mice.^[2] Absence of the natural ovastacin antagonist fetuin-B causes female infertility. Hence, this study could pave the way for the development of a novel treatment strategy for female infertility using small-molecule inhibitors based on an elaborated peptidomimetic scaffold.

Experimental Section

Homology modelling: Human ovastacin: Chain A of the *Danio rerio* hatching enzyme (PDB ID: 3LQB) and the FASTA sequence of human ovastacin (Q6HA08) were aligned with MOE (v2016.0802; Protein Align 2016.11), resulting in a sequence identity of 46.7%. During the modeling process the number of independent main-chain models was set to 100. Electrostatic solvation energy (Generalised Born/Volume Integral, GB/VI) was calculated and scored for refinements and the subsequent selection of the final model. Finally, the template structure was superposed to the ovastacin model and the Zn^{2+} -ion was copied to the model structure as new chain. For comparisons, pairwise RMSD values

were calculated and for examination of the model geometry, Ramachandran plots (Φ – Ψ plots) were visualized. For murine ovastacin the FASTA sequence Q6HA09 was employed and also aligned to PDB ID: 3LQB with MOE (v2018.01; Protein Align 2018.01). The resulting pairwise identity equals 44.5%. The final murine ovastacin model was generated and selected according to the remaining modeling steps described for human ovastacin.

Docking For the molecular docking of compound **6** the homology model of murine ovastacin was used as receptor. The docking procedure was set up in MOE (v2019.0102) and performed with GOLD (v5.7.1). The active site was defined by the Zn^{2+} ion. The ligand was used in its deprotonated form. The search efficacy was set to 100%, ChemScore was used as scoring function and 30 docking runs were performed. The resulting solutions were visually inspected and solutions lacking an interaction between hydroxamate and the zinc ion were discarded. The remaining 19 solutions were subjected to Postdock^[20] (postdock-1.2.svl script available via the CCG svl exchange server: svl.chemcomp.com) to create the figures and visualize the docking solutions according to their RMSD from the top ranked solution and their respective docking score.

Inhibition assay The inhibitory activity of tertiary amine hydroxamate inhibitors against mouse ovastacin was determined *in vitro* by means of a fluorogenic enzyme activity assay as previously described.^[5] Ovastacin was expressed as previously described^[6] and activated by human plasmin (Haematologic Technologies Inc., Essex Junction, USA) for 30 min in a molar ratio of 10:1. Concentration of active ovastacin (1 nM) was determined by titration and IC_{50} calculation with heterologously expressed murine fetuin-B.^[4] All assays were performed as independent double measurements in triplicate at 37 °C in 100 μ L final volume, buffered with 150 mM NaCl, 50 mM Tris-HCl, pH 7.4, 0.01% Brij-35. All hydroxamate inhibitors were dissolved in dimethyl sulfoxide. Enzyme activity measurements were started by addition of 25 μ M Ac-R–E(Edans)-D–R–Nle–V–G–D–D–P–Y–K(Dabcyl)-NH₂ ($K_m = 34 \pm 2.2$ μ M), dissolved in dimethyl sulfoxide (final concentration 1.4%). Initial velocities were recorded for at least 1000 s (50 times for 100 ms at intervals of 20 s). Thereafter, 1.5 μ L of proteinase K (at 20 mg/mL; Sigma–Aldrich) were added to reach complete substrate turnover, which was monitored and subsequently calculated using the formula $v = [S] \times m / \Delta F$, where $[S]$ is the substrate concentration, m the $[F/t]$ slope of initial linear substrate turnover, and ΔF the maximum fluorescence intensity corresponding to complete turnover. Kinetic parameters of inhibition (K_i^{app}) were determined by using Morrison's equation.^[21] K_i^{app} was used to enable comparison of data obtained by different batches of ovastacin with varying enzyme concentration. The mode of inhibition is yet unknown. However, small molecule inhibitors of astacin proteinases tend to exhibit mixed-type inhibition.^[22] Hence, K_i values were not calculated by simple conversion of K_i^{app} .

Supporting Information: Inhibition data of meprins, sequence alignments, compound characterization, homology models.

Acknowledgements

We are grateful to Antje Hamann, Mercedes Scharfe (IZI-MWT), Dr. Andrea Porzel (Leibniz Institute of Plant Biochemistry, Halle) and Dr. Christian Ihling (Martin-Luther-University Halle-Wittenberg) for their excellent technical support. Open access funding enabled and organized by Projekt DEAL.

Conflict of Interest

The authors declare no conflict of interest.

Keywords: astacins · hydroxamate · *in vitro* fertilization · infertility · metalloproteinase · metzincins · ovastacin

- [1] F. X. Gomis-Rüth, S. Trillo-Muyo, W. Stöcker, *Biol. Chem.* **2012**, *393*, 1027–1041.
- [2] A. D. Burkart, B. Xiong, B. Baibakov, M. Jiménez-Movilla, J. Dean, *J. Cell Biol.* **2012**, *197*, 37–44.
- [3] H. Körschgen, M. Kuske, K. Karmilin, I. Yiallourous, M. Balbach, J. Floehr, D. Wachten, W. Jahnen-Dechent, W. Stöcker, *Mol. Hum. Reprod.* **2017**, *23*, 607–616.
- [4] K. Karmilin et al., *Sci. Rep.* **2019**, *9*, 546.
- [5] A. Cuppari et al., *IUCrJ* **2019**, *6*, 317–330.
- [6] E. Dietzel et al., *Dev. Cell* **2013**, *25*, 106–112.
- [7] C. Gnoth, E. Godehardt, P. Frank-Herrmann, K. Friol, J. Tigges, G. Freundl, *Hum. Reprod.* **2005**, *20*, 1144–1147.
- [8] E. Dietzel, J. Floehr, E. van de Leur, R. Weiskirchen, W. Jahnen-Dechent, *Mol. Hum. Reprod.* **2017**, *23*, 25–33.
- [9] a) J. Floehr, E. Dietzel, J. Neulen, B. Rösing, U. Weissenborn, W. Jahnen-Dechent, *Hum. Reprod.* **2016**, *31*, 630–637; b) L. Fang, X. Hu, L. Cui, P. Lv, X. Ma, Y. Ye, *J. Assist. Reprod. Genet.* **2019**, *36*, 1101–1107.
- [10] a) C. Broder, C. Becker-Pauly, *Biochem. J.* **2013**, *450*, 253–264; b) D. Ramsbeck, A. Hamann, D. Schlenzig, S. Schilling, M. Buchholz, *Bioorg. Med. Chem. Lett.* **2017**, *27*, 2428–2431; c) E. D. Turtle, W.-B. Ho, *Expert Opin. Ther. Pat.* **2005**, *14*, 1185–1197.
- [11] D. Ramsbeck, A. Hamann, G. Richter, D. Schlenzig, S. Geissler, V. Nykiel, H. Cynis, S. Schilling, M. Buchholz, *J. Med. Chem.* **2018**, *61*, 4578–4592.
- [12] K. Tan, C. Jäger, D. Schlenzig, S. Schilling, M. Buchholz, D. Ramsbeck, *ChemMedChem* **2018**, *13*, 1619–1624.
- [13] T. Guevara, H. Körschgen, A. Cuppari, C. Schmitz, M. Kuske, I. Yiallourous, J. Floehr, W. Jahnen-Dechent, W. Stöcker, F. X. Gomis-Rüth, *Sci. Rep.* **2019**, *9*, 14683.
- [14] A. Mac Sweeney, S. Gil-Parrado, D. Vinzenz, A. Bernardi, A. Hein, U. Bodendorf, P. Erbel, C. Logel, B. Gerhartz, *J. Mol. Biol.* **2008**, *384*, 228–239.
- [15] J. L. Arolas, C. Broder, T. Jefferson, T. Guevara, E. E. Sterchi, W. Bode, W. Stöcker, C. Becker-Pauly, F. X. Gomis-Rüth, *Proc. Natl. Acad. Sci. USA* **2012**, *109*, 16131–16136.
- [16] C. Becker-Pauly, O. Barre, O. Schilling, U. auf dem Keller, A. Ohler, C. Broder, A. Schütte, R. Kappelhoff, W. Stöcker, C. M. Overall, *Mol. Cell. Proteomics* **2011**, *10*, M111.009233.
- [17] a) F. Grams, V. Dive, A. Yiotakis, I. Yiallourous, S. Vassiliou, R. Zwillig, W. Bode, W. Stöcker, *Nat. Struct. Biol.* **1996**, *3*, 671–675; b) I. Yiallourous, S. Vassiliou, A. Yiotakis, R. Zwillig, W. Stöcker, V. Dive, *Biochem. J.* **1998**, *331*, 375–379.
- [18] M.-N. Kruse, C. Becker, D. Lottaz, D. Köhler, I. Yiallourous, H.-W. Krell, E. E. Sterchi, W. Stöcker, *Biochem. J.* **2004**, *378*, 383–389.
- [19] J. Prox, P. Arnold, C. Becker-Pauly, *Matrix Biol.* **2015**, *44–46*, 7–13.
- [20] E. A. Wiley, G. Deslongchamps, *Comput. Visual Sci.* **2009**, *12*, 1–7.
- [21] J. F. Morrison, *Biochim. Biophys. Acta* **1969**, *185*, 269–286.
- [22] a) F. Madoux, C. Tredup, T. P. Spicer, L. Scampavia, P. S. Chase, P. S. Hodder, G. B. Fields, C. Becker-Pauly, D. Minond, *Biopolymers* **2014**, *102*, 396–406; b) A. Schulze, M. Wermann, H.-U. Demuth, T. Yoshimoto, D. Ramsbeck, D. Schlenzig, S. Schilling, *Anal. Biochem.* **2018**, *559*, 11–16.

Manuscript received: June 8, 2020

Accepted manuscript online: June 17, 2020

Version of record online: July 2, 2020